arXiv:1404.4503v2 [math.NA] 21 May 2014

Timestep control for weakly instationary flows

Christina Steiner and Sebastian Noelle

Abstract We report on recent work on adaptive timestep control for weakly instationary gas flows [16, 18, 17] carried out within SFB 401, TPA3. The method which we implement and extend is a space-time splitting of adjoint error representations for target functionals due to Süli [19] and Hartmann [10]. In this paper, we first review the method for scalar, 1D, conservation laws. We design a test problem for weakly instationary solutions and show numerical experiments which clearly show the possible benefits of the method. Then we extend the approach to the 2D Euler equations of gas dynamics. New ingredients are (i) a conservative formulation of the adjoint problem which makes its solution robust and efficient, (ii) the derivation of boundary conditions for this new formulation of the adjoint problem and (iii) the coupling of the adaptive time-stepping with the multiscale spatial adaptation due to Müller [12, 3], also developed within SFB 401. The combined space-time adaptive method provides an efficient choice of timesteps for implicit computations of weakly instationary flows. The timestep will be very large in regions of stationary flow, and becomes small when a perturbation enters the flow field. The efficiency of the Euler solver is investigated by means of an unsteady inviscid 2D flow over a bump.

1 Introduction

For the aeroelastic problems studied in the SFB 401 project both the stationary and the instationary case are of interest. In either case, *adaptive spatial grids* are well-

Christina Steiner
Institut für Geometrie und Praktische Mathematik, RWTH Aachen University, Templergraben 55, D-52056 Aachen, Germany. e-mail: steiner@igpm.rwth-aachen.de

Sebastian Noelle
Institut für Geometrie und Praktische Mathematik, RWTH Aachen University, Templergraben 55, D-52056 Aachen, Germany. e-mail: noelle@igpm.rwth-aachen.de

established and help to reduce computational time and storage. There has been a tremendous amount of research designing, analyzing and implementing codes which are adaptive in space, see e.g. [4, 12, 11, 13] and references therein.

Adaptive time-marching towards the stationary solution is an essential ingredient of most CFD codes. Here the timestep-sizes are adapted to the local CFL numbers. So far, it is not well-understood if adaptive timesteps might be useful for instationary flows. In the present paper we report on the work of SFB 401's project TPA3b, where we explored *adaptive explicit/implicit timesteps* for *weakly instationary flows*.

While time accuracy is still needed to study phenomena like aero-elastic interactions, large timesteps may be possible when the perturbations have passed. For explicit calculations of instationary solutions to hyperbolic conservation laws, the timestep is dictated by the *CFL* condition due to Courant, Friedrichs and Lewy [5], which requires that the numerical speed of propagation should be at least as large as the physical one. For implicit schemes, the *CFL* condition does not provide a restriction, since the numerical speed of propagation is infinite. Depending on the equations and the scheme, restrictions may come in via the stiffness of the resulting nonlinear problem. These restrictions are usually not as strict as in the explicit case, where the *CFL* number should be below unity. For implicit calculations, *CFL* numbers of much larger than 1 may well be possible. Therefore, it is a serious question how large the timestep, i.e. the *CFL* number, should be chosen.

Some time adaptation stategies developed by other authors are those of Ferm and Lötstedt [9] based on timestep control strategies for ODEs, and extended to fully adaptive multiresolution finite volume schemes, see [7, 6]. Alternatively Kröner and Ohlberger [11, 13] based their space-time adaptivity upon Kuznetsov-type a-posteriori L^1 error-estimates for scalar conservation laws.

In this paper we will use a space-time-split adjoint error representation to control the timestep adaptation. For this purpose, let us briefly summarize the space-time splitting of the adjoint error representation, see [8, 1, 2, 19, 10] for details. The error representation expresses the error in a target functional as a scalar product of the finite element residual with the dual solution. This error representation is decomposed into separate spatial and temporal components. The spatial part will decrease under refinement of the spatial grid, and the temporal part under refinement of the timestep. Technically, this decomposition is achieved by inserting an additional projection. Usually, in the error representation, one subtracts from the dual solution its projection onto space-time polynomials. Now, we also insert the projection of the dual solution onto polynomials in time having values which are H^1 functions with respect to space.

This splitting can be used to develop a strategy for a local choice of timestep. In contrast to the results reported in [19, 10] for scalar conservation laws we now investigate weakly instationary solution to the 2D Euler equations. The timestep will be very large in regions of stationary flow, and becomes small when a perturbation enters the flow field.

Besides applying well-established adjoint techniques to a new test problem, we further develop a new technique (first proposed by the authors in [18]) which simplifies and accelerates the computation of the dual problem. Due to Galerkin orthog-

onality, the dual solution φ does not enter the error representation as such. Instead, the relevant term is the difference between the dual solution and its projection to the finite element space, $\varphi - \varphi_h$. In [18] we showed that it is therefore sufficient to compute the spatial gradient of the dual solution, $w = \nabla\varphi$. This gradient satisfies a conservation law instead of a transport equation, and it can therefore be computed with the same conservative algorithm as the forward problem [18]. The great advantage is that the conservative backward algorithm can handle possible discontinuities in the coefficients robustly.

A key step is to formulate boundary conditions for the gradient $w = \nabla\varphi$ instead of v. Generally the boundary conditions for the dual problem come from the weighting functions of the target functional, e.g. lift or drag. To formulate boundary conditions for w which are compatible with the target functional, one has to lift the well-established techniques of characteristic decompositions from the dual solution to its gradient. We will present details on that in Section 4.

Starting with a very coarse, but adaptive spatial mesh and *CFL* below unity, we establish timesteps which are well adapted to the physical problem at hand. The scheme detects stationary time regions, where it switches to very high *CFL* numbers, but reduces the timesteps appropriately as soon as a perturbation enters the flow field.

We combine our time-adaptation with the spatial adaptive multiresolution technique [12]. The paper is organized as follows. We start with a brief description of the fluid equations and their discretization by implicit finite volume schemes, see Section 2. The adjoint error control is presented in Section 3, including a complete error representation (Section 3.2) and a related space-time splitting (Section 3.3). Section 4 contains the conservative approach to the dual problem und its boundary conditions. In Section 5 we present the adaptive method in time. In Section 6 we present the instationary test case, a 2D Euler transonic flow around a circular arc bump in a channel. In Section 7 results of the fully implicit and a mixed explicit-implicit time adaptive strategy are presented to illustrate the efficiency of the scheme. In Section 8 we summarize our results.

We refer the reader to [16, 18, 17] for further details and references.

Acknowledgement: We would like to thank Ralf Hartmann and Mario Ohlberger for stimulating discussions.

2 Governing equations and finite volume scheme

We will work in the framework of hyperbolic systems of conservation laws in space and time,

$$U_t + \nabla \cdot f(U) = 0 \quad \text{in } \Omega_T. \tag{1}$$

Here $\emptyset \subset \mathbb{R}^d$ is the spatial domain with boundary $\Gamma := \partial\emptyset \subset \mathbb{R}^d$ and $\Omega_T = \Omega \times [0,T) \subset \Omega \times \mathbb{R}^0_+$ is the space-time domain with boundary $\Gamma_T := \partial\Omega_T \subset \Omega \times \mathbb{R}^0_+$. U is

the vector of conservative variables and f the array of the corresponding convective fluxes f_i, $i = 1,\dots,d$, in the ith coordinate direction. Our prime example are the multi-dimensional Euler equations of gas dynamics.

We prescribe boundary conditions on the incoming characteristics as follows:

$$P_-(U^+)\,(\mathbf{f}_\nu(U^+) - g) = 0 \quad \text{on } \Gamma_T. \tag{2}$$

Here $\mathbf{f}(U) := (f(U), U)$ is the space-time flux, ν the space-time outward normal to Ω_T, and $\mathbf{f}_\nu(U) := \mathbf{f}(U)\cdot\nu$ the space-time normal flux. U^+ is the interior trace of U at the boundary Γ_T (or any other interface used later on). Given the boundary value U^+ and the corresponding Jacobian matrix $\mathbf{f}_\nu{}'(U^+)$, let $P_-(U^+)$ be the $(d+2)\times(d+2)$-matrix which realizes the projection onto the eigenvectors of $\mathbf{f}_\nu{}'(U^+)$ corresponding to negative eigenvalues. Then the matrix-vector product $P_-(U^+)\,\mathbf{f}_\nu(U^+)$ is the incoming component of the normal flux at the boundary, and it is prescribed in (2). See [17] for details.

We approximate (1)–(2) by a first or second order finite volume scheme with implicit Euler time discretization. The computational spatial grid Ω_h is a set of open cells V_i such that

$$\bigcup_i \overline{V_i} = \overline{\Omega}.$$

The intersection of the closures of two different cells is either empty or a union of common faces and vertices. Furthermore let $\mathcal{N}(i)$ be the set of cells that have a common face with the cell i, ∂V_i the boundary of the cell V_i and for $j \in \mathcal{N}(i)$ let $\Gamma_{ij} := \partial V_i \cap \partial V_j$ be the interface between the cells i and j and n_{ij} the outer spatial normal to Γ_{ij} corresponding to cell i. Since we will work on curvilinear grids, we require that the geometric consistency condition

$$\sum_{j\in N(i)} |\Gamma_{ij}| n_{ij} = 0 \tag{3}$$

holds for all cells.

Let us define a partition of our time interval $I := (0,T)$ into subintervals $I_m = [t_{m-1}, t_m]$, $1 \le m \le N$, where

$$0 = t_0 < t_1 < \ldots < t_m < \ldots < t_N = T.$$

The timestep size is denoted by $\Delta t_m := t_m - t_{m-1}$. Later on this partition will be defined automatically by the adaptive algorithm. We also denote the space-time cells and faces by $V_i^m := V_i \times I_m$ and $\Gamma_{ij}^m := \Gamma_{ij} \times I_m$, respectively. Given this space-time grid the implicit finite volume discretization of (1) can be written as

$$U_i^m + \frac{\Delta t_m}{|V_i|} \sum_{j\in\mathcal{N}(i)} |\Gamma_{ij}|\, F_{ij}^m = U_i^{m-1} \quad \text{for } m \ge 1. \tag{4}$$

It computes the approximate cell averages U_i^m of the conserved variables on the new time level. For interior faces Γ_{ij}, the canonical choice for the numerical flux is

a Riemann solver,

$$F_{ij}^m := F_{riem}(U_{ij}^m, U_{ji}^m, n_{ij}) \tag{5}$$

consistent with the normal flux $f_n(U) = f(U) \cdot n_{ij}$. In the numerical experiments in Section 7 we choose Roe's solver [15]. If $\Gamma_{ij} \subset \partial\Omega_T =: \Gamma_T$, then we follow the definition of a weak solution and define the numerical flux at the boundary by

$$F_{ij}^m := P_+(U_{ij}^m)\,\mathbf{f}_{\nu_{ij}}(U_{ij}^m) + P_-(U_{ij}^m)\,g_{ij}^m, \tag{6}$$

where g_{ij}^m is the average of g over Γ_{ij}^m.

For simplicity of presentation we neglect in our notation that due to higher order reconstruction the numerical flux usually depends on an enlarged stencil of cell averages.

3 Adjoint error control - adaptation in time

In order to adapt the timestep sizes we use a method which involves adjoint error techniques. We have applied this approach successfully to Burgers' equation in [18], and to the Euler equations of gas dynamics in [17].

Since a finite volume discretization in space and a backward Euler step in time are a special case of a Discontinuous Galerkin discretization, techniques based on a variational formulation can be transferred to finite volume methods.

The key tool for the time adaptive method is a space-time splitting of adjoint error representations for target functionals due to Süli [19] and Hartmann [10]. It provides an efficient choice of timesteps for implicit computations of weakly instationary flows. The timestep will be very large in time regions of stationary flow, and become small when a perturbation enters the flow field.

3.1 Variational Formulation

In this section we rewrite the finite volume method as a Galerkin method, which makes it easier to apply the adjoint error control techniques.

Let us first introduce the space-time numerical fluxes. Let $V_i^m = V_i \times I_m \in \Omega_{T,h}$ be a space-time cell, and let $\gamma \subset \partial V_i^m$ be one of its faces, with outward unit normal ν. There are two cases: if ν points into the spatial direction, then $\gamma = \Gamma_{ij} \times I_m$ and $\nu = (n, 0)$. If it points into the positive time direction, then $\gamma = V_i \times \{t_m\}$, and $\nu = (0, 1)$. Now we define the space-time flux by

$$\mathscr{F}_\nu^m(U_h) = \begin{cases} F_{ij}^m \text{ from (5)} & \text{if } \nu = n_{ij} \text{ and } \gamma \in \mathscr{E}_{T,h}^{int} \\ F_{ij}^m \text{ from (6)} & \text{if } \nu = n_{ij} \text{ and } \gamma \in \mathscr{E}_{T,h}^{ext} \\ (1-\theta)U_i^{m-1} + \theta U_i^m & \text{if } \nu = (0,1) \text{ and } m \geq 1 \\ U_i^0 & \text{if } \nu = (0,1) \text{ and } m = 0 \end{cases} \tag{7}$$

where $\mathscr{E}_{T,h}^{int}$ are the interior faces and $\mathscr{E}_{T,h}^{ext}$ the boundary faces. In the third case, $\theta \in [0,1]$, so the numerical flux in time direction is a convex combination of the cell averages at the beginning and the end of the timestep. Different values of θ will yield different time discretizations, e.g. explicit Euler for $\theta = 0$, implicit Euler for $\theta = 1$.

Let $\mathscr{V}_h := W^{1,\infty}(\Omega_{T,h})$ be the space of piecewise Lipschitz-continuous functions. Now we introduce the semi-linear form N by

$$\begin{aligned} N: \quad & \mathscr{U} \times \mathscr{V}_h \to \mathbf{R} \\ N(U,\varphi) := & \sum_{i,m} (\mathscr{F}_\nu^m(U), \varphi)_{\partial V_i^m} \\ & - \sum_{i,m} \Big((U, \varphi_{h,t})_{V_i^m} + (f(U), \nabla\varphi)_{V_i^m}. \Big) \end{aligned} \tag{8}$$

Here and below the sum is over the set $\{(i,m) \,|\, V_i^m \in \Omega_{T,h}\}$, i.e. all gridcells. Now we rewrite the finite volume method (4) as a first order Discontinuous Galerkin method (DG0):

$$\text{Find } U_h \in \mathscr{V}_h^0 \quad \text{such that} \quad N(U_h, \varphi_h) = 0 \qquad \forall \varphi_h \in \mathscr{V}_h^0, \tag{9}$$

where $\mathscr{V}_h^0$ is the space of piecewise constant functions over $\Omega_{T,h}$.

Remark 1. For the DG0 method, $U_h, \varphi \in \mathscr{V}_h^0$ are piecewise constant, so the last two terms in (9), containing derivatives of φ, disappear. Moreover, due to the geometric condition (3)

$$\sum_{\{j \,|\, \Gamma_{ij}^m \subset \partial V_i^m\}} \mathbf{f}(U_i^m) \cdot \nu_{ij}^m = 0$$

holds for all cells V_i^m. Therefore, the DG0 solution may be characterized by: Find $U_h \in \mathscr{V}_h^0$ such that

$$\sum_{i,m} (\mathscr{F}_\nu^m(U) - \mathbf{f}_\nu(U^+), \varphi_h)_{\partial V_i^m} = 0 \qquad \forall \varphi_h \in \mathscr{V}_h^0. \tag{10}$$

This form is convenient to localize our error representation later on.

3.2 Adjoint error representation for target functionals

In this section we define the class of target functionals $J(U)$ treated in this paper, state the corresponding adjoint problem and prove the error representation which we will use later for adaptive timestep control.

Before we derive the main theorems, we would like to give a preview of an important difference between error representations for linear and nonlinear hyperbolic conservation laws. For linear conservation laws (and many other linear PDE's), it is possible to express the error in a user specified functional,

$$\varepsilon_J := J(U) - J(U_h), \tag{11}$$

as a computable quantity η, so

$$\varepsilon_J = \eta \tag{12}$$

(see e.g. [1, 17, 20] and the references therein). In general, η will be an inner product of the numerical residual with the solution of an adjoint problem. Below we will see that such a representation does not hold for nonlinear hyperbolic conservation laws. The nonlinearity will give rise to an additional error ε_Γ^- on the inflow boundary, an error ε_Γ^+ on the outflow boundary, and a linearization error ε_Ω in the interior domain:

Theorem 1. *Suppose $\varphi \in \mathscr{V}$ solves the approximate adjoint problem*

$$\partial_t \varphi + \tilde{A}^T \nabla \varphi = \psi \qquad \text{in } \Omega_T, \tag{13}$$

$$\tilde{P}_+^T(\varphi - \psi_\Gamma) = 0 \qquad \text{on } \Gamma_T, \tag{14}$$

where $\tilde{A} := A(U_h)$. Let

$$\begin{aligned}
\varepsilon_\Gamma^- &:= -((P_-(U^+) - P_-(U_h^+))g, \varphi)_{\Gamma_T} \\
\varepsilon_\Gamma^+ &:= -(P_+(U^+)\mathbf{f}_\nu(U^+) - P_+(U_h^+)\mathbf{f}_\nu(U_h^+), \varphi - \psi_\Gamma)_{\Gamma_T} \\
\varepsilon_\Omega &:= (f(U) - f(U_h) - \tilde{A}(U - U_h), \nabla\varphi)_{\Omega_T}
\end{aligned}$$

and

$$\eta := N(U_h, \varphi) = N(U_h, \varphi - \varphi_h). \tag{15}$$

Then

$$\varepsilon_J + \varepsilon_\Gamma^- + \varepsilon_\Gamma^+ + \varepsilon_\Omega = \eta. \tag{16}$$

Our adaptation is based on computing and equidistributing this η. Typical examples for the functional J are the lift or the drag of a body immersed into a fluid. To simplify matters we consider functionals of the following form:

$$J(U) = (U, \psi)_{\Omega_T} - (P_+(U^+)\mathbf{f}_\nu(U^+), \psi_\Gamma)_{\Gamma_T}, \tag{17}$$

where ψ and ψ_Γ are weighting functions in the interior of the space-time domain Ω_T and at the boundary Γ_T. For the proof of Theorem 1 as well as an illustrative example of the functional J we refer again to [17].

For the adjoint problem (13) and (14) the role of time is reversed and hence $\tilde{P}_+$ plays the role of P_- in (2). Here ψ_Γ comes from the weighting function in the functional (17).

3.3 Space-time splitting

The error representation (16) is not yet suitable for time adaptivity, since it combines space and time components of the residual and of the difference $\varphi - \varphi_h$ of the dual solution and the test function. The main result of this section is an error estimate whose components depend either on the spatial grid size h or the timestep k, but never on both. The key ingredient is a space-time splitting of (16) based on L^2-projections. Similar space-time projections were introduced previously in [10, 19]. In [18] we adapted them to the finite element spaces and space-time Discontinuous Galerkin methods of arbitrary order.

The splitting takes the form

$$\eta = \eta_k + \eta_h. \tag{18}$$

For brevity, we only present the details for first-order finite volume schemes for which we obtain

$$\eta_k = \frac{\Delta t_m}{2} \sum_{i,m} \left((1-\theta)(U_i^{m-1} - U_i^{m-2}) + \theta(U_i^m - U_i^{m-1}), \psi - \tilde{A}^T w \right)_{V_i} \tag{19}$$

(we set $U_i^{-1} = U_i^0$ in the first summand). Thus our temporal error indicator is simply a weighted sum of time-differences of the approximate solution U_h, and the weights can be computed from the data ψ and the solution w of the conservative dual problem (21).

In our adaptive strategy, we will use the localized indicators

$$\bar{\eta}_k^m := \frac{1}{2} \sum_i \left| ((1-\theta)(U_i^{m-1} - U_i^{m-2}) + \theta(U_i^m - U_i^{m-1}), \psi - \tilde{A}^T w)_{V_i} \right|. \tag{20}$$

In the next section we present an example for the boundary conditions for the dual problem.

4 The conservative dual problem

In this section we present the conservative approach to the dual problem, which we introduced in [18] and derive boundary conditions for the gradient of the dual problem.

The adjoint equation (13) is a system of linear transport equations with discontinuous coefficients. Therefore, numerical approximations may easily become unstable. Another inconvenience is that in order to obtain a meaningful error representation in (16), the approximate adjoint solution φ should not be contained in $\mathscr{V}_h^0$. Therefore, φ is often computed in the more costly space $\mathscr{V}_h^1$.

In [18] we have proposed a simple alternative which helps to avoid both difficulties. Instead of computing the dual solution φ we will compute its gradient

$$w := \nabla\varphi,$$

which is the solution of the conservative dual problem

$$w_t + \nabla(\tilde{A}^T w) = \nabla\psi \quad \text{in } \Omega_T. \tag{21}$$

This system is in conservation form, and therefore it can be solved by any finite volume or Discontinuous Galerkin scheme. Moreover, (21) may be solved in $\mathscr{V}_h^0$, since a piecewise constant solution w already contains crucial information on the gradient of φ.

The scalar problem treated in [18] was set up in such a way that the characteristic boundary conditions for the dual problem became trivial. In [17] we developed boundary conditions for the more general initial boundary value problem (1) – (2).

Denoting the flux in (21) by $H := \tilde{A}^T w$, the boundary condition (14) becomes

$$\tilde{P}_+^T (H - H_\Gamma) = 0 \quad \text{on } \Gamma_T, \tag{22}$$

i.e. we prescribe the incoming component $\tilde{P}_+^T H$. Here H_Γ is a given real-valued vector function, which depends on ψ_Γ. However, this characteristic boundary condition needs to be interpreted carefully. Using (21) and denoting the interior trace at the flux by H_{int}, we may introduce the boundary flux by

$$H := \tilde{P}_-^T H_{int} + \tilde{P}_+^T H_\Gamma \quad \text{on } \Gamma_T.$$

Note that all the projections $\tilde{P}_\pm$ used below depend on the point $(x,t) \in \Gamma_T$ via the outside normal vector $\nu(x,t)$. The value $\tilde{P}_-^T H_{int}$ may be assigned from the trace w_{int} at the interior of the computational domain,

$$\tilde{P}_-^T H_{int} = \tilde{P}_-^T (\tilde{A}^T w)_{int}.$$

The boundary values $\tilde{P}_+^T H_\Gamma$ are computed using the PDE

$$\varphi_t = -H + \psi \tag{23}$$

with boundary values (14),

$$\begin{aligned}\tilde{P}_+^T H_\Gamma &= \tilde{P}_+^T \left(-\varphi_t + \psi\right)|_\Gamma \\ &= -(\tilde{P}_+^T \psi_\Gamma)_t + \tilde{P}_+^T \psi \\ &\approx -\frac{1}{\Delta t_m}\left(\tilde{P}_+^{T,m} \psi_\Gamma^m - \tilde{P}_+^{T,m-1} \psi_\Gamma^{m-1}\right) + \tilde{P}_+^{T,m-1} \psi. \end{aligned} \tag{24}$$

This completes the definition of the numerical boundary conditions for the conservative dual problem.

5 Adaptive concept

Now we combine the multiscale approach in space [12] and the time adaptive method derived from the space-time splitting of the error representation to get a space-time adaptive algorithm:

- solve the primal problem (1) on a *coarse* adaptive spatial grid (e.g. level $L = 2$) using uniform *CFL* numbers ($CFL = 0.8$),
- compute the dual problem (13) and (14) and the space-time-error representation (18). In particular, compute the localized error indicators $\bar{\eta}_k^m$ using (20).
- compute the new adaptive timestep sizes depending on the temporal part of the error representation and the *CFL* number on the new grid, aiming at an equidistribution of the error,
- solve the primal problem using the new timestep sizes on a *finer* spatial grid (e.g. level $L = 2$).

The advantage is, that the first computations of the primal problems and the dual problem are done on a coarse spatial grid, and therefore have low cost. These computations provide an initial guess of the timesteps for the computation on the finer spatial grid. We will restrict the timestep size from below to $CFL = 0.8$, since smaller timestep sizes only add numerical diffusion to the scheme and increase the computational cost. Note that all physical effects already have to be roughly resolved on the coarse grid in order to determine a reliable guess for the timesteps on the fine grid.

We will deal with some aspects in detail in the numerical examples in Section 7.

5.1 Asymptotic decay rates

Since the adaptive strategy outlined in Section 5 above depends on assumptions on the assymptotic behavior of the error, we first try to estimate these decay rates. There is no analytical result which shows how the error terms $\bar{\eta}_k$ and $\bar{\eta}_h$ depend on k and h.

Therefore, we estimate this dependence numerically. We compute a perturbed shock of Burgers equation, for details see [18]. We compare the two approaches:

- refinement only time
- and refinement only space.

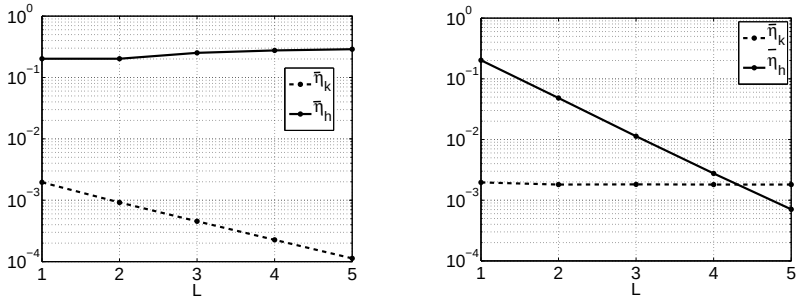

Fig. 1 Error representation for Burgers equation, first order method, $\bar{\eta}_k$ and $\bar{\eta}_h$ versus level of refinement. Left: uniform refinement in time. Right: uniform refinement in space

L	$\bar{\eta}_k$	$\bar{\eta}_h$	η_k	η_h	$J(u_h)$	$\eta_h+\eta_k$	θ
1	1.96e-03	2.02e-01	1.29e-04	2.00e-01	1.72e+00	2.01e-01	5.57e+00
2	9.81e-04	4.83e-02	1.83e-05	4.75e-02	1.74e+00	4.75e-02	5.49e+00
3	4.81e-04	1.21e-02	3.57e-06	1.17e-02	1.75e+00	1.17e-02	5.71e+00
4	2.37e-04	3.10e-03	1.30e-06	2.89e-03	1.75e+00	2.89e-03	7.06e+00

Table 1 Efficiency $\theta = \frac{\eta_h+\eta_k}{J(u)-J(u_h)}$ of the error representation, $CFL = 0.8$.

Each of the plots in Figure 1 show the error estimators $\bar{\eta}_k$ (error in time) and $\bar{\eta}_h$ (error in space). In the Figure 1(a) we refined only in time. Here the spatial error remains constant, while the time error still decreases with first order. The second Figure 1(b) shows the refinement only in space. The time error $\bar{\eta}_k$ is almost constant, while the spatial error is decreasing with second order.

Numerically the terms $\bar{\eta}_t$ and $\bar{\eta}_h$ behave as expected. They depend either on k or on h, but never on both. The behaviour of η_h and η_k is very similar, and not displayed here.

Remark 2. The numerically validated results can be used for adaptive grid refinement. The error estimator $\bar{\eta}_h$ can be used as an indicator for spatial adaption and the estimator $\bar{\eta}_k$ for time step control.

6 Setup of the numerical experiment

An instationary variant of a classical stationary 2D Euler transonic flow [14], is investigated to illustrate the efficiency of the adaptive method.

Steady state configuration. First we consider the classical setup in the stationary case. The computational domain is a channel of $3m$ length and $2m$ height with an arc bump of $l = 1m$ secant length and $h = 0.024m$ height cut out, see Figure 2. At the inflow boundary, the Mach number is 0.85 and a homogeneous flow field characterized by the free-stream quantities is imposed. At the outflow boundary, characteristic boundary conditions are used. We apply slip boundary conditions across the solid walls, i.e., the normal velocity is set to zero. In the numerical examples in Section 7 the height of the channel is $2m$ and the length $6m$.

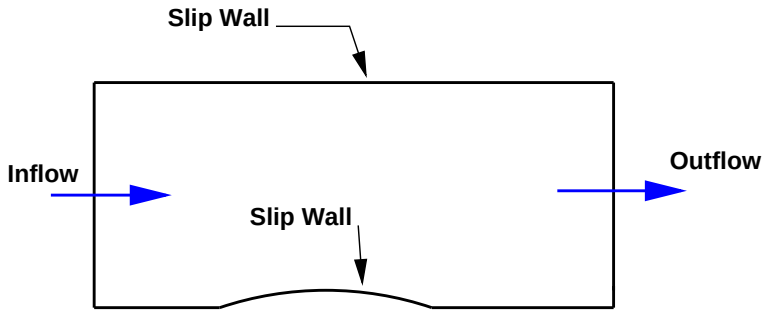

Fig. 2 Circular arc bump configuration of the computational domain Ω.

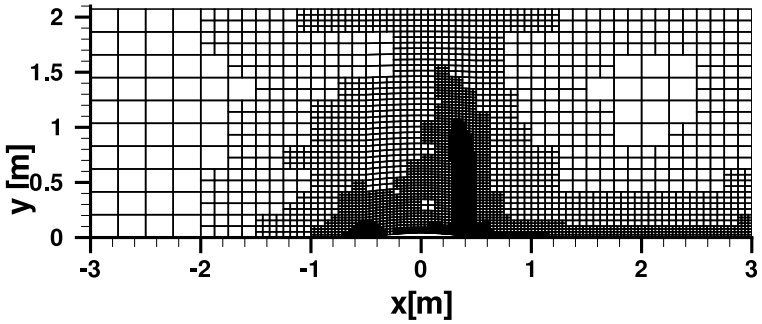

Fig. 3 Adaptive grid $L = 5$, to steady state solution in Figure 4 of the circular arc bump configuration.

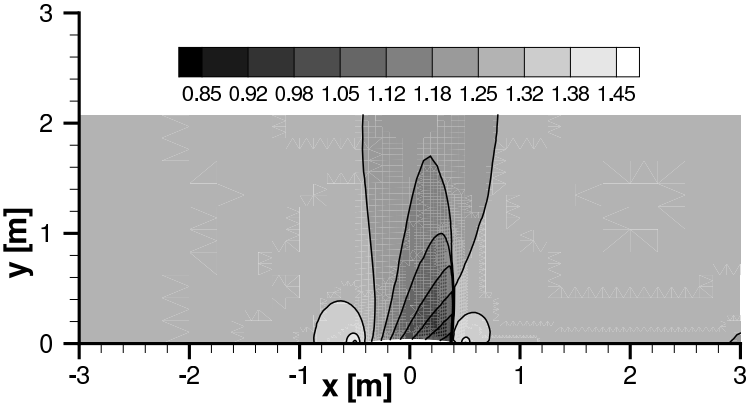

Fig. 4 Steady state solution of the circular arc bump configuration: Isolines of the density, $L = 5$.

The threshold value in the grid adaptation step for the multiscale analysis is $\varepsilon = 1 \times 10^{-3}$ and computations are done on adaptive grids with finest level $L = 2$ and $L = 5$ respectively. In general, a smaller threshold value results in more grid refinement whereas a larger value gives locally coarser grids.

In the stationary case at Mach 0.85 there is a compression shock separating a supersonic and a subsonic domain. The shock wave is sharply captured and the stagnation areas are highly resolved, see Figures 3 and 4.

We will use this steady state solution as initial data for the instationary test case.

Instationary test case. Now we define our instationary test case prescribing a time-dependent perturbation coming in at the inflow boundary. First we keep the boundary conditions fixed, and prescribe the corresponding stationary solution as initial data. Then we introduce for short time periods perturbations of the pressure at the left boundary. The first perturbation is about 20 percent of the pressure at the inflow boundary and the second 2 percent, see Figure 5. The perturbations imposed move through the domain and leave it at the right boundary. Then the solution is stationary again, see Figure 6. The total time is $t = 0.029s$. The formulas of the pertubations are given in detail in [17].

The first computation is done on an adaptive grid with finest level $L = 2$. We also compute the dual solution and the error representation on this level. Using the time-space-split error representation (18) we derive a new timestep distribution aiming at an equidistribution of the error. Finally this is modified by imposing a *CFL* restriction from below.

We aim to equidistribute the error and prescribe a tolerance $Tol(5) = 2^{-3}\bar{\eta}_k^{ref}$, where $\bar{\eta}_k^{ref}$ is the temporal error from the computation on level $L = 2$.

For this set-up we will show that the adaptive spatial refinement together with the time-adaptive method will lead to an efficient computation. The multiscale method provides a well-adapted spatial representation of the solution, and the dual solu-

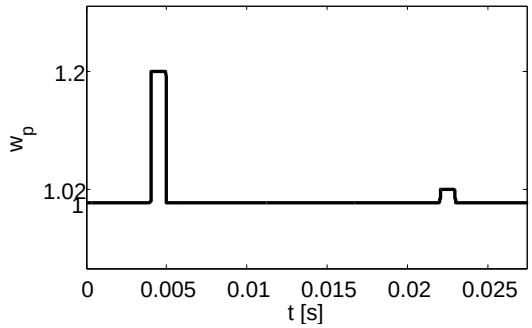

Fig. 5 Weighting function of the perturbation. $p_{in}(t) = p_\infty w_p(t)$

tion will detect time-domains where the solution is stationary. In these domains, the equidistribution strategy will choose large timesteps.

Target Functional. Now we set up the target functional. The functional $J(U)$ is chosen as a weighted average of the normal force component exerted on the bump and at the boundaries before and behind the bump:

$$J(U) = \sum_{i=1}^{7} \int_0^T \int_{\kappa_i} p\, \psi_i(x,y) ds \tag{25}$$

with

$$\kappa_i = \{(x,y) \in \Gamma : x \in [x_i - 0.25, x_i + 0.25]\}$$
$$\psi_i(x) = (x - (x_i - 0.25))^2 (x + (x_i + 0.25))^2 / 0.25^4, \quad x \in \kappa_i.$$

Here Γ is only the bottom part of Γ. In all computations presented in this section the functional (25) is chosen, which is the pressure averaged at several points at the bump in front and behind the bump. The x-coordinates of these points at the bottom are x_i = -3, -2, -1, 0, 1, 2, 3. At each of these points x_i a smooth function ψ_i is given with support $x_i - 0.25, x_i + 0.25$. This functional measures the pressure locally.

In Figure 6 we show a time-sequence of the instationary test case computed with uniform $CFL = 1$ on an adaptive grid with finest level $L = 5$. Note that the perturbation entering at the left boundary and moving through the boundary is resolved very well.

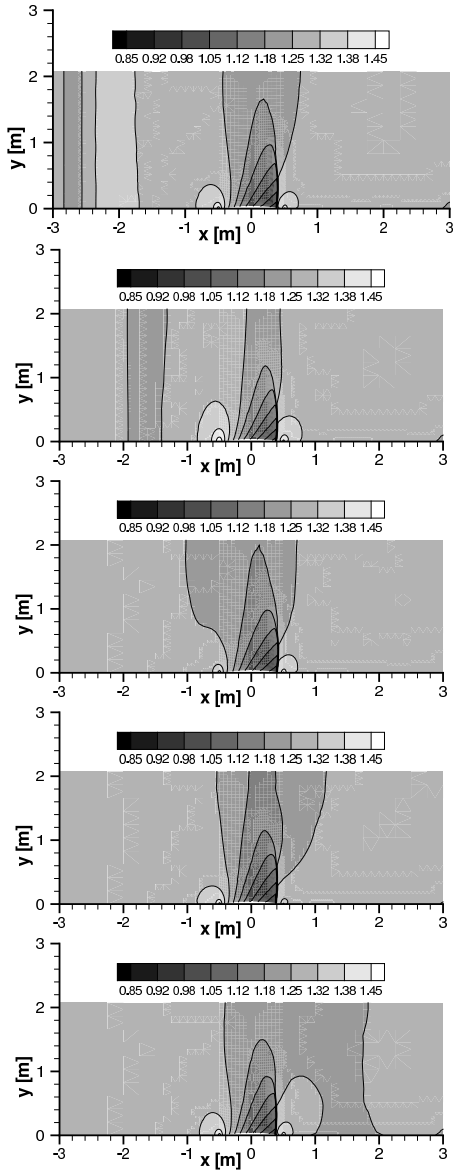

Fig. 6 Instationary solution of the circular arc bump configuration, uniform timestep $CFL = 1$, adaptive spatial grid on level $L = 5$, isolines of the density, perturbation entering on the left and leaving on the right side of the computational domain, from top to bottom: t = 0.0057s, 0.00912s, 0.01254s, 0.01596s, 0.01938s.

7 Computational results

7.1 Numerical strategies

We gave an outline of the adaptive method in Section 5. Now we will present numerical computations, where we compare some variations of the adaptive concept.

The first strategy is the one we proposed in [18]: We first compute a forward solution on a coarse grid ($L = 2$) and solve the adjoint problem on the adaptive grid of the forward solution. Then we use the information of the error representation based on the dual solution to determine a new sequence of timesteps. This sequence is used in the computation of the forward solution on a grid with finest level $L = 5$, where we additionally restrict the *CFL* number from below. We compare the results of the time adaptive strategy with uniform timestep distributions.

In the second strategy we modify the fully implicit timestepping strategy and introduce a mixed *implicit/explicit* approach. The reason is that implicit timesteps with $CFL < 5$ are not efficient, since we have to solve a nonlinear system of equations at each timestep. Thus, for $CFL < 5$, the new implicit/explicit strategy switches to the cheaper and less dissipative explicit method with $CFL = 0.5$.

We want to compare these strategies with respect to the following main aspects:

- What is the quality and what are the costs determining the adaptive timestep sequence from computations on the coarse grid?
- Is the predicted adaptive timestep sequence well-adapted to the solution on the fine grid?
- How is the solution affected if we use uniform timesteps larger than the predicted adaptive timestep sequence?

In order to quantify the results we have to compare with a reference solution. Since the exact solution is not available we perform a computation with $L = 5$ refinement levels using implicit timestepping with $CFL = 1$ amd explicit timestepping with $CFL = 0.5$.

7.2 Strategy I: Fully implicit computational results

7.2.1 Adjoint indicator and adaptive timesteps

Now we use the error representation on finest level $L = 2$ for a new time adaptive computation on finest level $L = 5$.

The first computation is done on a mesh with finest level $L = 2$. We compute until time $T = 0.0285s$, which takes 1000 timesteps with $CFL = 1$. We use the results of the error representation of this computation to compute a new timestep distribution. The forward problem takes $329s$ and the dual problem including the evaluation of the error representation $619s$ on an Opteron 8220 processor at 2.86 GHz. The total

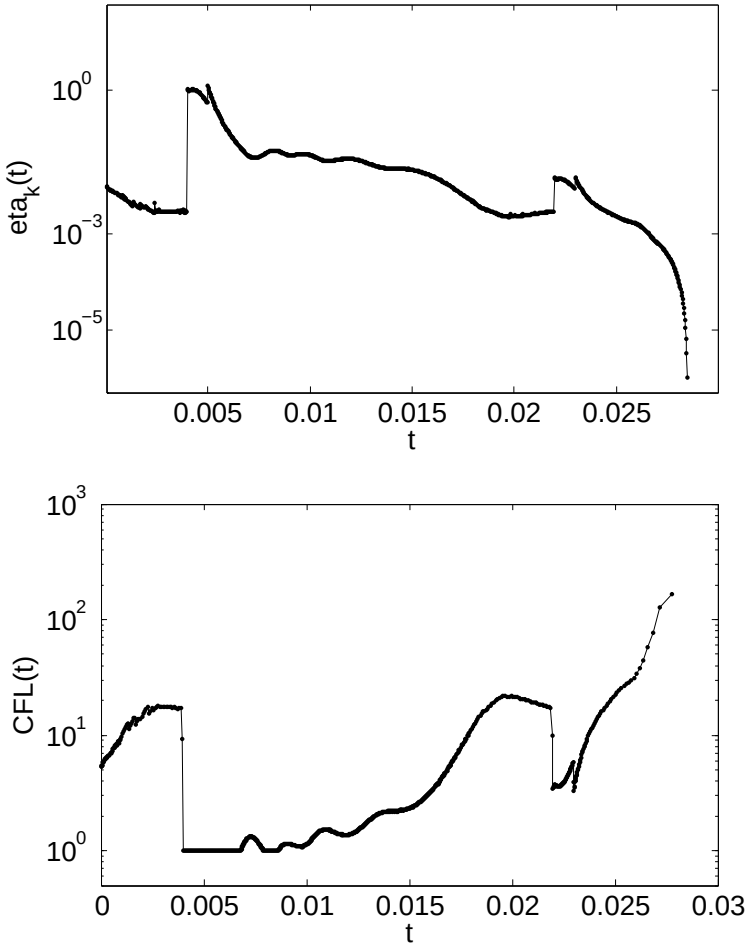

Fig. 7 Time component of the error representation $\bar{\eta}_k^m$(top) and new timesteps with *CFL* restriction from below $CFL(t_n)$ (bottom).

computational costs are 948*s*, and in memory we have to save 1000 solutions (each timestep) of the forward problem which corresponds to 48 MB (total). This gives us a new sequence of adaptive timesteps for the computation of level $L = 5$. The error indicator and the new timesteps are presented in Figure 7. In time intervals where the solution is stationary, i.e. at the beginning, and after the perturbations have left the computational domain, the timesteps are large. In time intervals where the solution is instationary we get well-adapted small timesteps.

Then we use the adaptive timestep sequence for a computation on level $L = 5$ and compare it with a uniform in time computation using $CFL = 1$. The uniform computation needs 8000 timesteps and the computational time is 21070*s*. The time adaptive solution is computed with 2379 timesteps and this computation takes 9142*s*.

In Figure 8 we show a sequence of plots of the uniform, $CFL = 1$ computation on an adaptive spatial grid with finest level $L = 5$. In Figure 8 we compare the pressure distribution at the bottom boundary of the uniform solution and the time adaptive solution at several times. The two solutions on level $L = 5$ match very well.

Remark 3. In [17] we also did some comparisions of the adjoint indicator with some ad hoc indicators, which estimate the variation of the solution from one timestep to the following. While these indicators also detect whether the solution is stationary or not, they lead to computations which are in general more expensive but not more accurate. In particular, most timesteps are smaller than in the case with adaptation via adjoint problems.

One advantage may be that we do not need to compute a dual solution, which makes the computation of the variation indicator less expensive. But this is only a small advantage, since we compute the error indicators on a coarse mesh. On the other hand the ad-hoc indicator is more straight forward to implement.

Another approach was to choose the maximum jump of the solution in one cell, both weighted and not weighted with the size of the cell. This was an approximation to the L^∞-norm. This indicator is not very useful, since it turned out to be highly oscillatory.

7.2.2 Comparison with Uniform timesteps

In many instationary computations where no a-priori information is known, one reasonable choice is to use uniform *CFL* numbers. Therefore we compared the computation with adaptive implicit timesteps with implicit computations using uniform *CFL* numbers. In Section 7.2 we have already done a computation with uniform *CFL* number, $CFL = 1$, on a grid with $L = 2$, to get timestep sizes for an adaptive computation on a grid with $L = 5$. As a reference solution we also computed with uniform *CFL* number, $CFL = 1$, a solution of the problem on a grid with $L = 5$. Now we compare these computations with computations using higher uniform *CFL* numbers.

First we choose a uniform *CFL* number of approximately 3.2, which corresponds to 2500 timesteps. This equals roughly the number of timesteps in the adaptive method, and hence it should give a fair comparison. The uniform computation takes about $11509s$, more than the $9142s$ of the adaptive computation (see Table 2). In the uniform computation most of the timesteps are more expensive, since they need more Newton steps, and more steps for solving the linear problems. This shows that the understanding of the dynamics of the solution pays directly in the nonlinear and linear solvers. Moreover, it can be seen from Figure 8 that the quality of the solution is considerably worse than for the adaptive computation.

Another computation with *CFL* number 10 takes only $3290s$. However, as can be seen from Figure 8 the solution is badly approximated: In the beginning of the computation the solutions of the different methods match very well, which means that the inflow at the boundary is well-resolved. As time goes on, the solutions differ more and more. After the perturbation has passed the bump, the perturbations

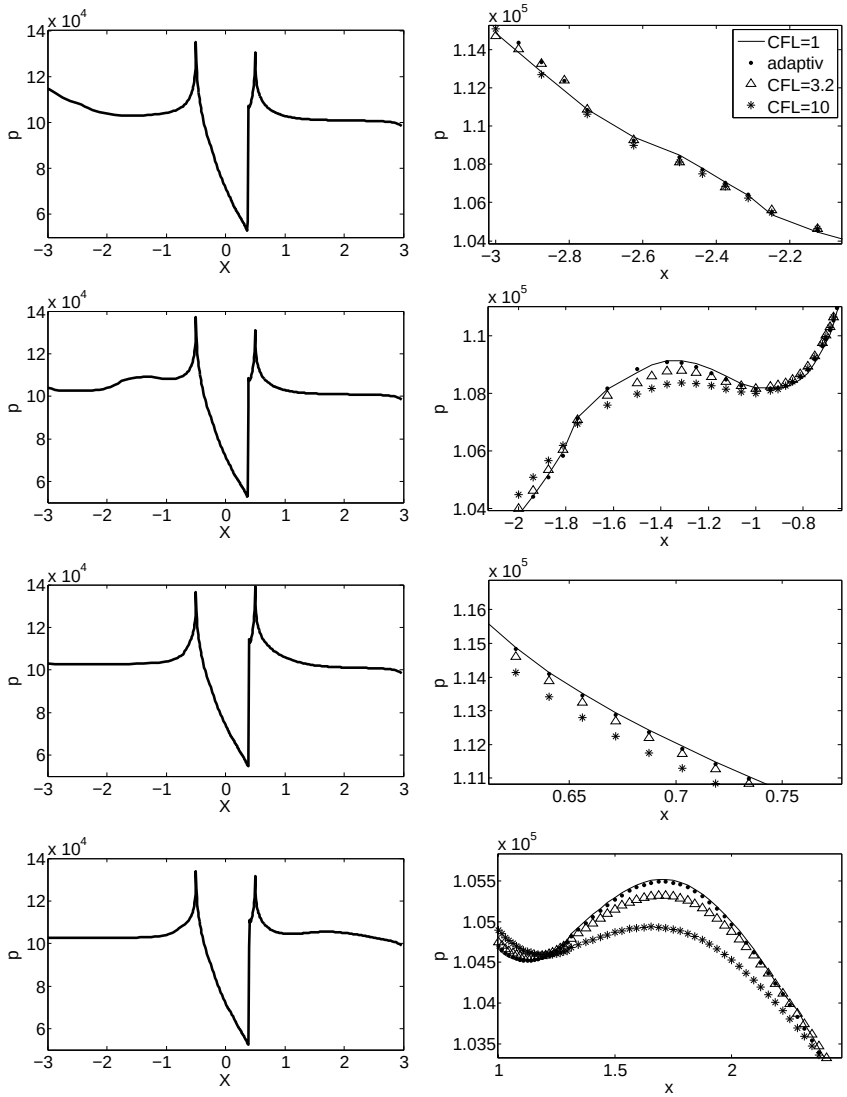

Fig. 8 Reference solution for 2D Euler equations: Left: adaptive spatial grid (finest level $L = 5$), uniform time steps ($CFL = 1$). Pressure p at bottom boundary at times t=0.005002, 0.007125, 0.009990, 0.011975, from top to bottom. Right: Zoom tracing the perturbations. Comparison of uniform timesteps with $CFL = 1,\ 3.2,\ 10$ and time-adaptive strategy.

differ strongly. Only the time-adaptive method approximates the reference solution ($CFL = 1$) closely.

Remark 4. Table 2 gives an overview of the CPU time and the number of Newton iterations and linear iterations for the computations. The costs for the computation of the indicator on level $L = 2$ are very low compared to the costs of computations on level $L = 5$. An adaptive computation including the computation of the indicator, i.e. $329s + 619s + 9142s$, is cheaper than the computation using uniform *CFL* number, e.g. $CFL = 1$, that needs $21070s$. Even the computation with $CFL = 3.2$ is more expensive than the time-adaptive computation, but leads to worse results, see Figure 8.

Table 2 shows that the CPU time is roughly proportional to the number of Newton iterations and not to the number of timesteps or linear solver steps. The CPU time is about $2.5s$ per Newton iteration. This means that we have to minimize the number of Newton iterations in total to accelerate the computation. This is done very efficiently by the time-adaptive approach. For a large range of *CFL* numbers from 1 to more than 100, it needs only one or two Newton iterations per timestep, without sacrificing the accuracy, see [17].

In this example, the stationary time regions are not very large compared to the overall computation. If the stationary regions were larger, the advantage of the time adaptive scheme would be even more significant.

	CPU [s]	timesteps	Newton steps	linear steps
adaptive timesteps	9142	2379	3303	16875
uniform $CFL = 1$	21070	8000	8282	32630
uniform $CFL = 3.2$	11509	2500	4904	26895
uniform $CFL = 10$	3290	800	1600	13500

Table 2 Performance for computations on $L = 5$ using different fully implicit timestepping strategies.

7.3 Strategy II: Explicit-implicit computational results

Now we modify the fully implicit timestepping strategy and introduce a mixed *implicit/explicit* approach. The reason is that implicit timesteps with $CFL < 5$ are not efficient, since we have to solve a nonlinear system of equations at each timestep. Thus, for $CFL < 5$, the new implicit/explicit strategy switches to the cheaper and less dissipative explicit method with $CFL = 0.5$. The timestep sequence is shown in Figure 9. Of course, we could choose variants of the thresholds $CFL = 0.5$ and 5.

As we can see in Table 7.3, the new strategy requires 5802 timesteps, where 95% are explicit. The CPU time of $7730s$ easily beats the fully explicit solver ($18702s$), and is also superior to the fully implicit adaptive scheme ($9142s$, see Table 2). The computational results are presented in Figure 10. The results of the combined explicit-implicit strategy are very close to the results of the fully explicit method, and far superior to all fully implicit methods. Note that the explicit scheme serves

as reference solution, since it is well-known that it gives the most accurate solution for an instationary problem.

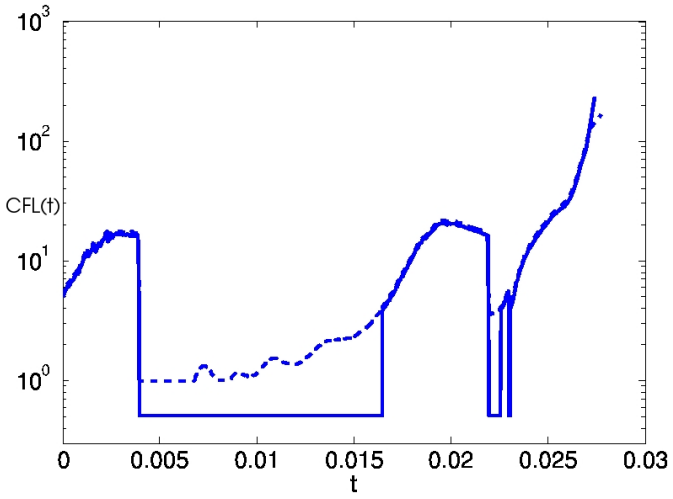

Fig. 9 2D Euler equations, comparison of timestep sequence derived from error representation for implicit computation (dashed line) and for mixed explicit-implicit computation (bold line).

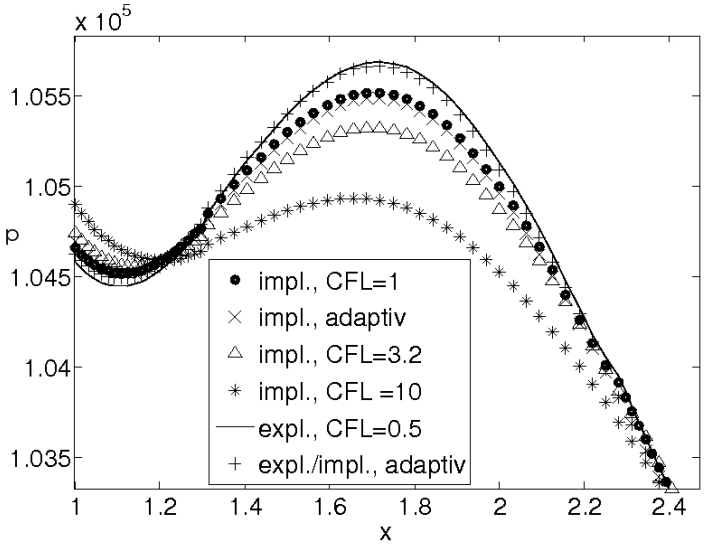

Fig. 10 2D Euler equations, comparison of solutions in time on adaptive grid with finest level $L = 5$, pressure p at the bottom boundary, zoom of the perturbation at time t=0.011975

	CPU [s]	timesteps (total)	timesteps (implicit)
explicit $CFL = 0.5$	18702	16000	-
adaptive expl.-impl.	7730	5802	259

Table 3 Performance for computations on $L = 5$ using fully explicit timesteps and the time-adaptive explicit-implicit strategy.

8 Conclusion

In the series of works [16, 18, 17] reviewed in this paper, explicit and implicit finite volume solvers on adaptively refined quadtree meshes have been coupled with adjoint techniques to control the timestep sizes for the solution of weakly instationary compressible inviscid flow problems.

For the 2D Euler equations we study a test case for which the time-adaptive method does reach its goals: it separates stationary regions and perturbations cleanly and chooses just the right timestep for each of them. The adaptive method leads to considerable savings in CPU time and memory while reproducing the reference solution almost perfectly.

Our approach is based upon several analytical ingredients: In Theorem 1 we state a complete error representation for nonlinear initial-boundary-value problems with characteristic boundary conditions for hyperbolic systems of conservation laws, which includes boundary and linearization errors. Besides building upon well-established adjoint techniques, we also add a new ingredient which simplifies the computation of the dual problem [18]. We show that it is sufficient to compute the spatial gradient of the dual solution, $w = \nabla\varphi$, instead of the dual solution φ itself. This gradient satisfies a conservation law instead of a transport equation, and it can therefore be computed with the same algorithm as the forward problem. For discontinuous transport coefficients, the new conservative algorithm for w is more robust than transport schemes for φ, see [18]. Here we also derive characteristic boundary conditions for the conservative dual problem, which we use in the numerical examples in Section 7.

In order to compute the adjoint error representation one needs to compute a forward and a dual problem and to assemble the space-time scalar product (20). Together, this costs about three times as much as the computation of a single forward problem. In our application, the error representation is computed on a coarse mesh ($L = 2$), and therefore it presents only a minor computational overhead compared with the fine grid solution ($L = 5$). In other applications, the amount of additional storage and CPU time may become significant.

For instationary perturbations of a 2D stationary flow over a bump, we have implemented and tested both a fully implicit and a mixed explicit-implicit timestepping strategy. The explicit-implicit approach switches to an explicit timestep with

$CFL = 0.5$ in case the adaptive strategy suggests an implicit timestep with $CFL < 5$. Clearly, the mixed explicit-implicit strategy is the most accurate and efficient, beating the adaptive fully implicit in accuracy and efficiency, the implicit approach with fixed *CFL* numbers in accuracy, and the fully explicit approach in efficiency.

References

1. Becker, R., Rannacher, R.: A feed-back approach to error control in finite element methods: basic analysis and examples. East-West J. Numer. Math. **4**(4), 237–264 (1996)
2. Becker, R., Rannacher, R.: An optimal control approach to a posteriori error estimation in finite element methods. Acta Numer. **10**, 1–102 (2001)
3. Bramkamp, F., Lamby, P., Müller, S.: An adaptive multiscale finite volume solver for unsteady and steady state flow computations. J. Comput. Phys. **197**(2), 460–490 (2004)
4. CLAWPACK: Conservation law package. http://www.amath.washington.edu/ claw/ (1998)
5. Courant, R., Friedrichs, K., Lewy, H.: Über die partiellen Differenzengleichungen der mathematischen physik. Math. Ann. **100**(1), 32–74 (1928)
6. Domingues, M., Gomes, S., Roussel, O., Schneider, K.: An adaptive multiresolution scheme with local time stepping for evolutionary PDEs. J. Comput. Phys. **227**(8), 3758–3780 (2008)
7. Domingues, M., Roussel, O., Schneider, K.: On space-time adaptive schemes for the numerical solution of PDEs. In: CEMRACS 2005—computational aeroacoustics and computational fluid dynamics in turbulent flows, *ESAIM Proc.*, vol. 16, pp. 181–194. EDP Sci., Les Ulis (2007)
8. Eriksson, K., Johnson, C.: Adaptive finite element methods for parabolic problems. IV. Nonlinear problems. SIAM J. Numer. Anal. **32**(6), 1729–1749 (1995)
9. Ferm, L., Lötstedt, P.: Space-time adaptive solution of first order PDEs. J. Sci. Comput. **26**(1), 83–110 (2006)
10. Hartmann, R.: A posteriori Fehlerschätzung und adaptive Schrittweiten- und Ortsgittersteuerung bei Galerkin-Verfahren für die Wärmeleitungsgleichung. Master's thesis, Universität Heidelberg (1998)
11. Kröner, D., Ohlberger, M.: A posteriori error estimates for upwind finite volume schemes for nonlinear conservation laws in multidimensions. Math. Comp. **69**(229), 25–39 (2000)
12. Müller, S.: Adaptive multiscale schemes for conservation laws, *Lecture Notes in Computational Science and Engineering*, vol. 27. Springer-Verlag, Berlin (2003)
13. Ohlberger, M.: A posteriori error estimate for finite volume approximations to singularly perturbed nonlinear convection-diffusion equations. Numer. Math. **87**(4), 737–761 (2001)
14. Rizzi, A., Viviand, H. (eds.): Numerical methods for the computation of inviscid transonic flows with shock waves, *Notes on Numerical Fluid Mechanics*, vol. 3. Friedr. Vieweg & Sohn, Braunschweig (1981)
15. Roe, P.L.: Approximate Riemann solvers, parameter vectors, and difference schemes. J. Comput. Phys. **43**(2), 357–372 (1981)
16. Steiner, C.: Adaptive timestepping for conservation laws via adjoint error representation. Ph.D. thesis, RWTH Aachen University, Germany (2008. http://darwin.bth.rwth-aachen.de/opus3/volltexte/2009/2679/)
17. Steiner, C., Müller, S., Noelle, S.: Adaptive timestep control for instationary solutions of the euler equations. submitted to SIAM J. Sci. Comput. (2009)
18. Steiner, C., Noelle, S.: On adaptive timestepping for weakly instationary solutions of hyperbolic conservation laws via adjoint error control. Comm. Numer. Meth. Eng., doi:10.1002/cnm.1183 (2008)
19. Süli, E.: A posteriori error analysis and adaptivity for finite element approximations of hyperbolic problems. In: An introduction to recent developments in theory and numerics for conservation laws (Freiburg/Littenweiler, 1997), *Lect. Notes Comput. Sci. Eng.*, vol. 5, pp. 123–194. Springer, Berlin (1999)

20. Süli, E., Houston, P.: Adaptive finite element approximation of hyperbolic problems. In: Error estimation and adaptive discretization methods in computational fluid dynamics, *Lect. Notes Comput. Sci. Eng.*, vol. 25, pp. 269–344. Springer, Berlin (2003)